Astron. Astrophys. 317, 273–289 (1997)

ASTRONOMY AND ASTROPHYSICS

Simulation of chemical reactions and dust destruction in protoplanetary accretion disks

I. Bauer[2], F. Finocchi[1], W.J. Duschl[1,2,3], H.-P. Gail[1], and J.P. Schlöder[2]

[1] Institut für Theoretische Astrophysik, Universität Heidelberg, Tiergartenstraße 15, D-69121 Heidelberg, Germany
[2] Interdisziplinäres Zentrum für Wissenschaftliches Rechnen der Universität Heidelberg, Im Neuenheimer Feld 368, D-69120 Heidelberg, Germany
[3] Max-Planck-Institut für Radioastronomie, Auf dem Hügel 69, D-53121 Bonn, Germany

Received 10 January 1996 / Accepted 2 May 1996

Abstract. This paper considers the gas phase chemistry in a protoplanetary accretion disk, especially the chemistry initiated in the gas phase by destruction of dust close to the central star.

Slow radial particle transport moves gas and dust from the cold outer parts of a protoplanetary accretion disk into its warm central part where chemical reactions in the gas phase are activated. At the same time gases frozen on the surface of dust grains are vaporized and later the dust grains themselves are vaporized or destroyed by chemical surface reactions. These processes initiate a rich chemistry in the protoplanetary accretion disk.

The simulation of chemical reactions, as in the case of an accretion disk, mostly leads to a large and stiff system of differential or differential-algebraic equations. For the integration of such systems implicit methods are required. We present an efficient BDF-method and give a detailed description of the error and stepsize control and the strategies to minimize the numerical effort of the linear algebra problems. Typical applications for chemical processes (chemistry and dust destruction) in an accretion disk are treated with this method. The corresponding code DAESOL turned out to be more robust and much faster than the more conventional code used first.

Some results for the chemistry in a protoplanetary accretion disk are briefly discussed.

Key words: accretion disks – molecular processes – solar system: formation – methods: numerical – dust

1. Introduction

It is generally thought that the process of star formation is initiated by a gravitational collapse in slowly rotating molecular cloud cores. Such a collapse quickly enhances centrifugal forces, giving rise to a highly flattened configuration, i.e. a disk or a solar nebula associated with a stellar embryo. The early protostar grows through rapid accretion of material out of the disk. While there is evidence that the formation of disks around pre-main-sequence objects is quite common (e.g., Beckwith and Sargent 1993, Strom et al. 1993), there is no clear observational evidence with respect to the final fate of the disk. Either the material dissipates after feeding the stellar embryo, or a second star or perhaps a brown dwarf is formed from the disk material (see Mathieu (1994) for a review) or, as we know at least for one single case a planetary system forms from the disk.

In this paper we are interested in this last case of a *protoplanetary accretion disk* from which at some late stage of the disks evolution planetary companions do form by a process which starts with assembling interstellar micron sized dust particles into millimeter to centimeter sized particles and which ends up after going through a hierarchy of several different accumulation processes with bodies of planetary size (see Lissauer 1993 for a review).

The evolution of the solar nebula principally can be divided into three stages (Cameron 1988). During the first stage, the *formation stage*, the protoplanetary disk is built up from infalling matter from a molecular cloud core. The formation time of the disk equals roughly the collapse time of the protostellar cloud of $\approx 10^5$ yr. In this stage, the disk mass may be large compared to the stellar mass since the central star has not yet accreted much of its final mass. The infalling matter passes a strong accretion shock standing at the surface of the disk where the gas and grains may be considerably processed (Neufeld and Hollenbach 1994). If the external supply of mass ceases the disk enters into the second stage, the *viscous stage*. In this stage internal torques, generated for instance by viscosity associated with convective flows, cause a redistribution of angular momentum within the disk. Mass is transported inwards and finally is incorporated into the sun while angular momentum is transported outwards causing a secular spread of the disk (Lynden-Bell and Pringle 1974). The ratio of disk mass to the protostellar mass is small and the scale height of the disk at every distance from the star

Send offprint requests to: H.-P. Gail

is small compared to the distance itself, i.e. the disk is geometrically thin. It is possible that heating of the disk surface by the sun suppresses convection and the accretion flow may cease entirely. The duration of this phase is of the order of a few 10^5 yr. In the third stage, the *clearing stage* the gaseous component of the nebula is dispersed, probably by powerful pre-main sequence stellar winds (Horedt 1978, Elmegreen 1978). This final stage lasts for less than $\approx 10^7$ yr (see Beckwith and Sargent 1993).

In this paper we concentrate on the viscous phase where the accretion rate is small (of the order of $10^{-7}\,M_\odot/\mathrm{yr}$) and feeding of the disk by infalling material has ceased. During this phase, planetary formation starts with agglomeration of dust particles. The molecular cloud material added to the disk during the first stage, which passed through a strong accretion shock and changes its chemical composition by dissociation and dust sublimation and subsequent reformation of molecules and condensates (Neufeld and Hollenbach 1994) has been accreted into the sun. The material forming the disk during the accretion phase has not passed through strong shocks and is likely to be nearly unprocessed material from the molecular cloud.

The chemistry in a protoplanetary disk during this phase has been discussed up to now on the basis of chemical equilibrium considerations (cf. the reviews of Prinn (1993) and van Dishoek et al. (1993) and references therein). While this may be correct in the warm and dense inner parts of the disk at distances of the order of 1 AU or less, this is unlikely to be true in the cold outer parts (Duschl et al. 1996). In this paper we calculate the chemical composition in the protoplanetary disk from reaction kinetics.

We determine the chemical composition in a gas element as it moves towards the centre. The physical state of the gas phase is calculated from a model for the accretion disk which is coupled to the chemistry of the gas and the dust. Due to the exponential temperature dependence of the chemical rate coefficients and the close coupling between temperature, opacity and dust evaporation the system of equations describing the problem is extremely stiff and highly nonlinear.

For the solution of the stiff and nonlinear system we use the integrator DAESOL (Bleser 1986, Eich 1987, Bauer 1994), a multistep-method with variable coefficients. DAESOL is not only suited for the solution of ordinary differential equations but also for linear implicit index 1 differential-algebraic equations of the following type

$$\begin{aligned} A(t,y,z)y &= f(t,y,z) \\ 0 &= g(t,y,z)\,. \end{aligned}$$

Emphasis is laid on the error and stepsize control, based on true variable grid formulas, allowing the order and step size to change in every step. We describe efficient monitor strategies that reduce the computational effort for evaluation and decomposition of the Jacobian matrix, used in the implicit multistep-method. The code DAESOL is compared with DDRIV3 (Kahaner et al. 1989) which is widely used in astrophysics and also based on BDF-formulas with variable coefficients, but with different strategies in error control and order and step size selection. We demonstrate that DAESOL is not only more robust but also much faster.

The plan of this paper is as follows: In Sects. 2 and 3 we briefly outline the accretion disk model and the basic equations for the chemistry of the gas phase. Sect. 4 describes the method used for calculating vaporization and dust destruction and the coupling of these processes to the gas-phase chemistry. Sect. 5 describes some assumptions for the model calculation. In Sect. 6 we illustrate a BDF-method and detail the special strategies used in the BDF-code DAESOL. Sect. 7 gives a short discussion of the results for the chemistry in the protoplanetary accretion disk.

2. Model of the accretion disk

A simple semi-analytical approach for the structure of a viscous thin protoplanetary accretion disk was discussed in Duschl et al. (1996, henceforth called paper I). Our calculation of the chemistry in the accretion disk is based on this simplified model. The basic equations for the disk structure are

$$\Sigma = 2500\,\frac{\mathrm{g}}{\mathrm{cm}^2}\; s^{-\frac{3}{5}} \tag{1}$$

$$h = 1.446\cdot 10^{12}\,\mathrm{cm}\; s^{\frac{21}{20}} \left(\frac{M}{M_\odot}\right)^{-\frac{3}{8}} \left(M_{-7}\,\kappa\right)^{\frac{1}{8}}\; \mu^{-\frac{1}{2}} \tag{2}$$

$$T = 997\,\mathrm{K}\; s^{-\frac{9}{10}} \left(\frac{M}{M_\odot}\right)^{\frac{1}{4}} \left(M_{-7}\,\kappa\right)^{\frac{1}{4}} \tag{3}$$

$$P = 71.65\,\frac{\mathrm{g}}{\mathrm{cm\ s}^2}\; s^{-\frac{51}{20}} \left(\frac{M}{M_\odot}\right)^{\frac{5}{8}} \left(M_{-7}\kappa\right)^{\frac{1}{8}}\; \mu^{-\frac{1}{2}} \tag{4}$$

where

$$M_{-7} = \frac{M}{10^{-7}\,M_\odot/\mathrm{yr}}\,. \tag{5}$$

The radial coordinate s is in units of astronomical units (AU). Σ is the surface density, h the (half) thickness of the disk, and P and T are the pressure and temperature in the midplane of the disk. κ is the mass absorption coefficient and μ the mean molecular weight. The opacity is determined by (i) the opacity of the gas, (ii) the opacity of the dust, and (iii) the opacity of ices, if present (see Sect. 5.1 for details). κ and μ depend on P and T.

The inwards directed drift velocity of the matter in the disk is

$$v_s = 26.94\,\frac{\mathrm{cm}}{\mathrm{s}}\; s^{-\frac{2}{5}}\, M_{-7}\,. \tag{6}$$

The radial position of a gas parcel, starting at s_0 at time $t = 0$ and drifting inwards with velocity v_s is

$$s^{1.4} = s_0^{1.4} - 2.52\cdot 10^{-12} M_{-7}\, t \tag{7}$$

at time t.

Table 1. Model parameters of the accretion disk used in the computation of disk structure

mass M	$1\,M_\odot$
mass-loss rate M	$10^{-7}\,M_\odot/\mathrm{yr}$
surface density Σ	2500 g/cm^2 at $s = 1$

The accretion disk shrinks with decreasing s. According to this, the slow radial inward drift of the gas in the accretion disk is accompanied by a vertical velocity component v_z given by

$$v_z = \frac{\partial h}{\partial s} \cdot v_s \sim \frac{z}{s} v_s \,. \tag{8}$$

For symmetry reasons v_z vanishes in the midplane. At a distance h over the midplane v_z equals the value given by (8). The z-gradient of v_z in the continuity equation is approximated, then, by

$$\frac{\partial v_z}{\partial z} \sim \frac{v_z}{h} \,. \tag{9}$$

This velocity is small enough not to disturb local hydrostatic equilibrium.

The total density of hydrogen nuclei (assuming all H to be in H_2 and an abundance of He of 0.1) is

$$N_\mathrm{H} = 8.68 \cdot 10^{14}\ \mathrm{cm}^{-3} \cdot s^{-\frac{33}{20}} \left(\frac{M}{M_\odot}\right)^{\frac{3}{8}} \left(M_{-7}\,\kappa\right)^{-\frac{1}{4}}\ \mu^{-\frac{1}{2}} \,. \tag{10}$$

The disk parameters used in the model calculations are listed in Table 1.

3. Chemistry in the accretion disk

Chemical processes in cosmical objects usually proceed far away from thermal equilibrium. In order to determine the chemical composition of such objects, a kinetic treatment of the possible reaction pathways leading to the different atomic and molecular species is necessary. For a protoplanetary accretion disk, it has been argued in paper I that in the dense and warm central parts of the disk the chemistry easily evolves into a chemical equilibrium state. An equilibrium calculation for the composition of the gas phase has, then, been performed for the central regions (where $s \leq 1$) but it is questionable, whether even in these dense inner regions of the disk the chemistry operates under chemical equilibrium conditions. Here we consider explicitly the reaction kinetics in the protoplanetary disk.

3.1. Equations for the gas-phase chemistry

The gas phase chemistry in the disk is determined by two–body and three–body reaction processes between neutral atomic and molecular species. Usually ternary reactions are inefficient in the chemistry of cosmic objects. For protostellar accretion disks, however, three-body reactions have to be considered at least for the hydrogen atoms and molecules in a simulation of the chemistry since (i) the density in the central part of the protoplanetary system is quite high and collisional de-excitation by a third particle during two particle collisions becomes efficient, and (ii) the available time for the system to evolve its chemistry is also long compared to the reaction timescales of ternary reactions. We do not take into account in this paper the different photoprocesses (dissociation, ionization) by UV radiation possibly emitted by the protosun because the disk is optically thick nor do we consider the ionization by cosmic radiation since this process is unlikely to be important in a protoplanetary disk (Dolginov and Stepinsky 1994). We also neglect the possibility of ionization by extinct radionuclides like Al^{26} or I^{129} which are known to have existed in the early planetary system (see, e.g., Swindle 1993) and may form the source for some ionization of the matter (Umebayashi and Nakano 1981).

The basic equation governing the number density of a specific atomic or molecular species is the continuity equation. If n_i denotes the particle density per unit volume of a given species i, the equation describing the time evolution of n_i without chemical reactions is

$$\frac{\partial n_i}{\partial t} + \nabla \cdot (n_i \boldsymbol{v}) = 0 \,. \tag{11}$$

For the accretion disk we adopt a cylindrical coordinate system with s denoting the radial distance from the protosun and z denoting the height over the midplane of the disk. The change of n_i along a streamline of the gas flow is

$$\frac{\mathrm{d}n_i}{\mathrm{d}t} = \frac{\partial n_i}{\partial t} + v_s \frac{\partial n_i}{\partial s} + v_z \frac{\partial n_i}{\partial z} \,. \tag{12}$$

We assume independence of all physical quantities on the azimuthal angular coordinate and add the contribution of the chemical reactions to Eq. (11). Then we obtain the following ordinary differential equation for n_i in the comoving frame

$$\begin{aligned} \frac{\mathrm{d}n_i}{\mathrm{d}t} &= -n_i \left(\frac{v_s}{s} + \frac{\partial v_s}{\partial s} + \frac{\partial v_z}{\partial z}\right) \\ &\quad -n_i \sum_j k_{ij} \cdot n_j + \sum_{jl} k_{ijl} \cdot n_j \cdot n_l \\ &\quad -n_i \sum_{jl} k_{ijl} \cdot n_j \cdot n_l + \sum_{jlm} k_{ijlm} \cdot n_j \cdot n_l \cdot n_m \end{aligned} \tag{13}$$

v_s and v_z are determined by the disk model, see Eqs. (6) and (9). The second term on the r.h.s. describes the loss of species i due to reactions between species i with species j. The third term represents the gain of species i due to reactions between species j and l and the fourth and fifth term describe the loss and production of species i due to three particle collisions, respectively. The k_{ij}, k_{ijl}, and k_{ijlm} are the rate coefficients of the corresponding reactions.

The rate coefficients are approximated as usual by the Arrhenius form

$$k = k_0 T^\alpha \exp\left(-\frac{E_a}{k_B T}\right) \,. \tag{14}$$

E_a is the activation energy barrier, k_0 and α are constants.

The differential equation (13) governs the time evolution of each species i in the mixture of atoms and molecules within a specific parcel of gas and we have such an equation for every species i. We obtain, then, a system of coupled nonlinear ordinary differential equations describing the time evolution of the chemistry in the comoving frame of a gas element. These equations have to be solved simultaneously with a set of algebraic equations for the disk structure. These are Eqs. (3) and (4) for the state of the gas, Eq. (7) for the actual radial position s of the gas parcel at each instant t and the equations determining the mean molecular weight μ and the opacity κ, which are specified later. Eqs. (3), (4) and (7) can be solved directly whereas the equations for the opacity κ and for the mean molecular weight μ are implicit. In mathematical language, we deal with a system of *Differential Algebraic Equations* (DAE), which requires special methods for its efficient solution, described in detail in Sect. 6.

3.2. The chemical reaction network

We consider in this paper the gas-phase chemistry of the four most abundant elements H, C, N and O. Helium is considered in some reactions as collision partner for dissociation or deexcitation. The chemical reaction network for the neutral-neutral gas phase reactions used in our calculation is that given by Mitchell (1984)[1]. The rates are updated, where possible, by the rates given in Baulch et al. (1992). The system of Mitchell is extended by some reactions given in Baulch et al. which are not contained in the list of Mitchell, but we only considered such reactions from Baulch et al. (1992) where either the determination of the corresponding backward reactions were possible or where the backward reaction is inefficient for energetic reasons.

The system of binary reactions is extended by the following ternary reactions of atomic and molecular hydrogen

$$\mathrm{H_2 + H + H \quad \longleftrightarrow \quad H_2 + H_2} \tag{15}$$

$$\mathrm{H + H + H \quad \longleftrightarrow \quad H + H_2\,.} \tag{16}$$

Rate coefficients for these reactions are taken from Baulch et al. 1992. Usually, three particle reactions need not to be taken into account if the densities of the species are as low as in the interstellar matter or in circumstellar shells. But this does not hold for the protoplanetary accretion where the particle density of hydrogen is very high up to a considerable distance from the protosun (at least up to some AU, cf. Eq. 10). The first reaction (15) is responsible for the formation of H_2 in the outermost parts of the disk, when almost all the available hydrogen is bound into H_2, keeping the abundance of free H atoms at a very low level. The second reaction (16) is important in the region where the molecular hydrogen starts to dissociate where it prevents a rapid complete dissociation.

The vaporization of silicate dust injects besides oxygen the molecule SiO and the atoms Fe and Mg into the gas phase (see paper I). The reaction network, for this reason, considers additionally the free atoms Si, Mg, and Fe and the molecule SiO. No other compounds of these elements are considered in this calculation. At high temperature the SiO is dissociated by collisional dissociation with hydrogen

$$\mathrm{SiO + H \quad \longrightarrow \quad Si + O + H} \tag{17}$$

$$\mathrm{SiO + H_2 \quad \longrightarrow \quad Si + O + H_2\,.} \tag{18}$$

The rate coefficients for this reactions are estimated from those of the similar CO collisional dissociation. The coefficient k_0 is assumed to be the same and the activation energy is set equal to the binding energy of SiO (E=8.28 eV). The rate coefficient for the two reactions is then assumed to be

$$k = 6 \cdot 10^{-9} \exp\left(-\frac{96000}{T}\right)\,.$$

Totally, our reaction network considers 450 reactions between 80 molecular species of the elements mentioned above.

4. Vaporization of ice and dust destruction

As in paper I we assume that the dust component consists of a mixture of carbon and iron-magnesium-silicate dust. In this paper we consider additionally the presence of H_2O and CO ice mantles on the dust grains. At the very low temperatures (10 . . . 200 K) prevailing in the outer regions of the disk any gaseous carbon monoxide and water vapor will freeze out on the surface of solid particles. Other sorts of ices are observed in the interstellar medium (Sandford & Allamandola, 1993) but these are not considered here, because they do not form major components of the ice mantles. We simply assume that the dust grains are coated by an inner H_2O–ice layer, which itself is embedded in an outer CO–ice layer. This corresponds to the assumption, that the ice mantles of all grains grew under the same conditions in the parent molecular cloud, from which the protostellar system has formed.

Our assumption is motivated by the fact that CO ice has the lowest vaporization temperature (about 30K) while H_2O vaporizes at about 150K. Laboratory measurements seem to indicate (Sandford and Allamandola 1988) that the CO may diffuse into the H_2O ice layer and form a mixed H_2O-CO ice which, then, may show a complex outgassing behaviour for the CO component during warming up the ice. We do not consider such complications in this paper.

The vaporization of the ices injects CO and H_2O molecules into the gas phase. This has not an immediate consequence on the chemistry, since vaporization of the ices occurs at such a low temperature, that the chemistry of the neutral molecules is effectively frozen in due to activation energy barriers. It does, however, increase the abundance of these molecules in the gas phase and later when the temperature raises to such a level that the neutral-neutral chemistry starts to operate, these molecules are involved in the gas phase chemistry.

The fundamental method for calculating the vaporization is outlined in paper I. We give here a brief explanation how this is

[1] Corrected for some misprints in that list.

coupled to the calculation of the gas phase chemistry. Consider the vaporization of a given species i (either CO or H_2O) from a grain surface. We denote by J_i^a the rate of attachment of the species i at the grain surface per unit time and unit surface area. This is given by

$$J_i^a = \alpha_i A n_i v_i \,. \tag{19}$$

n_i is the particle density in the gas phase,

$$v_i = \sqrt{\frac{kT}{2\pi m_i}} \tag{20}$$

its root mean square average thermal velocity[2], A the particle surface and α_i the sticking probability. The reverse process, i.e. the dissociation rate J_i^d, is given by

$$J_i^d = \alpha_i A v_i \frac{P_i^{eq}}{kT} \,. \tag{21}$$

P_i^{eq} denotes the partial pressure in chemical equilibrium of the species i. The net loss rate by vaporization is therefore

$$J_i = J_i^d - J_i^a = \alpha_i A v_i \big(\frac{P_i^{eq}}{kT} - n_i\big) \,. \tag{22}$$

The equation of change for the particle radius a is

$$\frac{\mathrm{d}a}{\mathrm{d}t} = V_0 \cdot \sum_i J_i \tag{23}$$

where

$$V_0 = \frac{A_m m_{\mathrm{H}}}{\rho_D} \tag{24}$$

is the volume occupied by the nominal molecule in the condensate. A_m is the molecular weight of the nominal molecule, m_{H} the hydrogen atom mass and ρ_D the bulk density of the solid. We then have

$$\frac{\mathrm{d}a}{\mathrm{d}t} = \sum_i \alpha_i V_0 v_i \big(n_i - \frac{P_i^{eq}}{kT}\big) \,. \tag{25}$$

The experimentally determined sticking coefficient of water at temperatures below 230 K is close to unity (Pruppacher & Klett 1978). We decided to use a value of $\alpha = 0.9$ in our calculation. The same value is used for CO. The density of ice at 150 K and below is slightly less than that at room temperature (Pruppacher & Klett 1978) but since this does not have much influence on the results, we simply use the data for room temperature. The vapor pressures of H_2O and CO over their ices are taken from Léger et al. (1985). More recent experimental values for latent heat of vaporization (Sandford & Allamandola 1988, 1993) seem to indicate slightly less values than that used in our calculation. The density of solid CO is from CRC-handbook (Weast & Astle 1982)[3]. The numerical values for the coefficients used in our calculation are listed in Table 2.

[2] Note that the rate (19) refers to unit surface area of the particle and not to unit cross section. The rate per unit cross section is higher by a factor of 4.

[3] To determine the influence of such parameters on the solution sensitivity analysis should be performed. DAESOL is already equipped with efficient tool for this task.

Table 2. Data used for calculating the vaporization of ices

substance	ρ_D[g/cm^2]	A	α	p_{vap}[dyn/cm^2]
H_2O	1	18.015	0.9	$P^{eq} = \mathrm{e}^{-6070/T+30.86}$
CO	1.25	28.01	0.9	$P^{eq} = \mathrm{e}^{-1030/T+27.37}$

Sources of Data see text.

The data used for the calculation of the destruction of the carbon and silicate dust grains are given in paper I.

Now we consider that we have an ensemble of dust grains with a broad size spectrum. We assume that all these particles have an inner ice mantle of H_2O of thickness $D_{\mathrm{H_2O}}$ and an outer ice mantle of CO of thickness D_{CO}. The central carbon or silicate dust grains which serve as the condensation centres for the ices are assumed to be spherical and to have the size distribution of the Mathis-Rumpl-Nordsieck dust model (MRN) (Mathis et al. 1977)

$$f(a)da = Ca^{-\frac{7}{2}}da \,.$$

We use $\log C = -15.20$ for carbon dust and $\log C = -15.14$ for silicate dust. This corresponds to a 100% condensation of Si into silicate grains and a 70% condensation of C into carbon grains. These values for C are slightly different from the values given by Mathis et al. (1977) because they used the element abundances given by Cameron (1973), whereas we use the abundances given by Anders & Grevesse (1989). The grains have sizes between a minimum size $a_{\mathrm{min}} = 0.005\,\mu$m and a maximum size $a_{\mathrm{max}} = 0.25\,\mu$m. Outside this interval, the distribution function $f(a)$ vanishes. $f(a)$ gives the number of grains per size interval and per hydrogen nucleus.

The MRN size distribution is not a really good approximation for the size spectrum of carbon and silicate dust grains in the protoplanetary accretion disk since it is known that in molecular cloud cores, from which new stars are formed, small grains are less abundant than predicted by the MRN model (e.g. Dorschner and Henning 1995). But this is not a real problem for the model calculation, since the vaporization of ices occurs close to equilibrium and in this case is independent of the number of grains and the thickness of their ice coatings.

Real grains with outer ice layers will not have the simple spherical structure assumed above, but a much more complicated structure due to agglomeration. However, nothing can be said at present about the real structure of icy grains in the protoplanetary accretion disk. For this reason we may take our model as a crude zero order approximation for treating the problem of ice vaporization.

The vaporization process is most conveniently described by the total change Δa of the particle radius during the past history up to the present instant. The equation for this quantity is

$$\frac{\mathrm{d}\Delta a}{\mathrm{d}t} = -\frac{\mathrm{d}a}{\mathrm{d}t} = -\sum_i \alpha_i V_0 v_i \big(n_i - \frac{P_i^{eq}}{kT}\big) \tag{26}$$

and this equation has to be solved subject to the initial condition $\Delta a = 0$ at some instant where vaporization has not yet occurred.

Equation (26) has to be integrated simultaneously with the equations for the chemistry and the disk model until Δa becomes equal to the original thickness $D_{\rm CO}$ or $D_{\rm H_2O}$, respectively. At this limit, the corresponding ice layer is completely vaporized and the equation (26) needs not to be integrated further. The vaporization of CO and H_2O are well separated in temperature. Thus, the two differential equations (26) for the two sorts of ice layers can be considered separately. Only one of these two equations has to be included in the calculations at one time.

The total volume of the water ice layer is after reduction of its original thickness $D_{\rm H_2O}$ by $\Delta a_{\rm H_2O}$

$$V_{\rm H_2O} = N_{\rm H}\,\frac{4}{3}C\int_{a_{\min}}^{a_{\max}} a^{-\frac{7}{2}}\,\cdot\,\left(a + D_{\rm H_2O} - \Delta a_{\rm H_2O}\right)^3\,da\,. \quad (27)$$

$N_{\rm H}$ is the particle density of hydrogen nuclei. Similar, the volume of the outer CO layer is given by

$$V_{\rm CO} = N_{\rm H}\,\frac{4}{3}C\int_{a_{\min}}^{a_{\max}} a^{-\frac{7}{2}}\cdot\left(a + D_{\rm H_2O} + D_{\rm CO} - \Delta a_{\rm CO}\right)^3\,da \quad (28)$$

A simple integration yields the volumes $V_{\rm H_2O}$ and $V_{\rm CO}$ as low order polynomials in Δa, from which they can easily be calculated. The change of the concentration n_i of CO or H_2O in the gas phase due to the vaporization of the ice layer is

$$\frac{{\rm d}n_i}{{\rm d}t} = -\frac{1}{V_0}\frac{{\rm d}V_i}{{\rm d}t} \quad (29)$$

(observe that V_i is reduced by the vaporization). V_0 is given by (24) and has to be calculated from the data of CO and H_2O. The r.h.s. of (29) has to be added as an additional rate term to the r.h.s. of Eq. (13) for CO and H_2O, respectively. This determines the increase of the density n_i of molecules from the vaporizing ice layer in the gas phase and this in turn determines the vaporization rate in Eq. (26).

In this way we have included the vaporization of ices in our model calculation.

The dust grains are destroyed at much higher temperatures. The basic processes are discussed in some detail in paper I. In this paper *vaporization* is the only destruction process for grains that is considered in the numerical simulation. In reality, chemical sputtering by OH is the dominating process for the carbon dust component, see Paper I and Lenzuni et al. (1995). The precise destruction process has only a marginal influence on the disk structure since carbon dust in any case is destroyed prior to silicate dust. As shown in paper I, only the destruction of the *last* dust component strongly modifies the disk structure.[4]

We include the vaporization of the two dust components in the model calculation in just the same way as we did for the vaporization of the ices. The reduction Δa of grain size due to vaporization is determined for both, the carbon and the silicate dust, by an equation of the form (26). The total volume of the dust grains after reduction of their size by Δa is

$$V_{\rm dust} = N_{\rm H}\,\frac{4}{3}C\int_{\max(a_{\min},\Delta a)}^{a_{\max}} a^{-\frac{7}{2}}\,\cdot\,(a-\Delta a)^3\,da\,. \quad (30)$$

The amount of vaporized material injected into the gas phase has again to be determined from Eq. (29). For the numerical simulation this changes the r.h.s. of the differential equations and there appears a discontinuity both in the equations for gas phase chemistry and in the equation for the change of grain radius when the last grains disappear. This has to be treated carefully in the numerical calculation.

The carbon injects mainly C_1 and C_3 and a small amount of a lot of other species into the gas phase (for details see paper I). For simplicity we have assumed that carbon is only injected as C atoms into the gas phase. The association of carbon from the gas phase is neglected in the case of carbon vaporization (see paper I and Lenzuni et al. 1995). This means, that in Eq. (26) the term proportional to n_i is neglected. Except for this, the details of the calculations are just the same as in the case of vaporization of ices.

For the silicate dust we assume that the dust decomposes into a number of small molecules since the nominal molecule $MgFeSiO_4$ of the solid silicate material does not exist as a free molecule. Due to the lack of thermochemical data for the iron-magnesium silicate we calculate the decomposition rate for the following reaction

$$Mg_2SiO_4 \quad\longrightarrow\quad 2Mg + SiO + 3O \quad (31)$$

which gives the dominating products for the decomposition of the pure magnesium silicate. One of the liberated magnesium atoms is counted as an Fe atom in the chemical rate equations. The change of the particle radius (26) is calculated from the effective vaporization rate of SiO molecules from the surface (see paper I). The injection rate for SiO into the gas phase is determined from the r.h.s. of Eq. (29) and this is added as an additional rate term to the r.h.s. of Eq. (13) for SiO. The corresponding rate terms in the Eqs. (13) for Mg and Fe are the same as that for SiO and the rate term in the equation for O is three times that of SiO. In this way we have calculated the decomposition of the silicate dust.

The main difference of the present treatment of silicate destruction compared to paper I is that we do not assume quasistationary decomposition as in paper I but treat it as a time dependent process, though in fact the numerical solution of the time dependent problem confirms that the decomposition process always operates close to a quasistationary equilibrium state.

5. Model calculation

5.1. The opacity

The mass absorption coefficient κ is approximated as in paper I as a linear superposition of the three components: gas, carbon dust and silicate dust. The contribution of the ice layers existing

[4] The precise process, however, strongly influences the details of the gas phase chemistry.

at low temperatures is neglected since this paper concentrates on the chemistry in the warm inner parts of the disk.

The gas opacity is set to the constant value $\kappa_{\rm gas} = 10^{-3}{\rm cm}^2\,{\rm g}^{-1}$. The dust opacity is calculated for the carbon and the silicate dust using the approximations of the small particle limit (see, for instance, Draine & Lee 1984) and the optical constants of Draine (1985). Rosseland mean opacities are calculated for each dust component separately and the mass absorption coefficient of the gas-dust mixture is set to

$$\kappa = \frac{\rho_{\rm carb}}{\rho}\kappa_{\rm carb} + \frac{\rho_{\rm sil}}{\rho}\kappa_{\rm sil} + \kappa_{\rm gas} \tag{32}$$

where $\rho_{\rm carb}$ and $\rho_{\rm sil}$ are the mass density of the carbon and silicon dust component in the gas-dust mixture and ρ the total mass density. Since the $\kappa_{\rm carb}$ and $\kappa_{\rm sil}$ are of the order of $100 \ldots 1000\,{\rm cm}^2 \cdot {\rm g}^{-1}$ and the mass fraction of the dust is of the order of 1%, the mass absorption coefficient of the mixture is of the order of $1\,{\rm cm}^2 \cdot {\rm g}^{-1}$. The assumed superposition of the opacities to obtain the Rosseland mean opacity of the mixture is not completely correct but should be of sufficient accuracy to study the effect of the opacity variations during grain destruction.

The opacity of the two dust components is strongly temperature dependent while the temperature given by (3) depends itself on the opacity. This results in a nonlinear coupling between the temperature structure in the disk and the opacity. This dependence is not strong, however, because κ enters with the fourth square root in Eq. (3). On the other hand, if more than 90% of the dust has been destroyed the temperature structure reacts strongly on the reduced opacity. This introduces a further and strongly nonlinear coupling between the problem of disk structure and chemistry, since the vaporization rate is extremely temperature dependent. This coupling poses a high nonlinearity for the numerical integration of the DAE–system.

5.2. Initial conditions

The elemental composition of the protoplanetary disk determines to a large extent its chemical state. There is no reason to suspect that the composition of the material with high angular momentum which collapsed to form the protoplanetary disk was different from low angular momentum material which directly fell into the central star. Thus, the element abundances in the disk are believed to be the same in the disk and in the proto-sun. We used in this calculation the solar system element abundances as derived by Anders and Grevesse (1989) from solar, terrestrial and meteoritic material.

As initial conditions for the gas phase chemistry, we prescribe the chemical composition of the gas at a radius s = 1 000 AU. In this paper we assume an initial mixture consisting of H_2, H, and N_2. Almost all of the available hydrogen is bound in H_2, only 1% is assumed to exist as free H-atoms. All carbon that is not bound in dust particles is bound in CO, which is frozen out on the surface of the dust grains. The oxygen in the molecular cloud gas is partially present as free O atoms and partially has formed H_2O molecules. If the infalling molecular cloud material passes the accretion shock close to the surface of the disk, the gas is heated and the oxygen reacts with the hydrogen to form H_2O (Neufeld and Hollenbach 1994). If the gas cools down again the water vapour condenses onto the grains. Thus we assume that all oxygen that is not bound into the silicate dust is in H_2O, which is frozen out on the surface of dust grains. All nitrogen is assumed to be in N_2.

This is a strong simplification of the chemical mixture which is expected to come from the parent molecular cloud into the accretion disk (Pollack et al. 1994). A lot of additional molecules are observed in dense star forming regions and especially some of the carbon should be in CH_3OH and some of the nitrogen is observed to have formed NH_3. The bulk of these elements, however, is in CO and N_2 and for simplicity we initially neglect all less abundant molecules in the gas phase since this most likely has no influence on the chemistry in the warm and dense inner portions of the disk.

A real protoplanetary disk is much smaller, typically only 100 AU (Ruden and Pollak 1991), than our choice of 1 000 AU for the radius where we started our inwards integration. We choose this bigger outer radius to achieve that the H/H_2 ratio has relaxed to a quasistationary equilibrium state before the gas enters into the region of real interest, since the true initial H/H_2 ratio is not known in advance.

6. The method of integration

The modeling of the chemistry in an accretion disk leads to initial value problems for systems of **O**rdinary **D**ifferential **E**quations (ODE), sometimes coupled to algebraic equations, then resulting in so-called **D**ifferential **A**lgebraic **E**quations (DAE).

The matter in the accretion disk undergoes huge temperature changes. The rate coefficients depend exponentially on the temperature, which varies from a few K to 2000 K or more. These huge changes make the integration, especially the last part, highly nonlinear. Simulation showed that the system is also very stiff, which means, that some chemical reactions are in the transient phase (the equilibrium point will be reached very soon) and others vary more slowly. The Jacobian of the right-hand side of the differential equations has then some large negative real eigenvalues. A fast and reliable solution of such systems requires solvers that are especially developed to cope with these difficulties.

For the integration of such stiff systems implicit methods – mostly multistep-methods – are used (for a survey see, e.g., Bock et al. 1995). Especially BDF-methods (**B**ackward **D**ifferentiation **F**ormulae) have proven to be very successful because of their good stability qualities (see, e.g., Brenan et al. 1989).

6.1. Backward differentiation formulae

BDF-methods are multistep-methods, based on polynomial interpolation of the last, already computed values. The formulas

have been developed first by Curtiss and Hirschfelder (1952) and have been applied to DAEs by Gear (1971).

First we want to introduce shortly the principles of BDF-methods. For the sake of lucidity we restrict to ordinary differential equations. Afterwards the principles are applied to DAEs and the special strategies in the BDF-code DAESOL are described.

In every step an explicit multistep-formula is used to compute an initial guess for the implicit corrector polynomial:

Considering the nonlinear ODE

$$y = f(t, y), \quad y(t_0) = y_0, \quad y \in I\!R^m, \tag{33}$$

the idea is to approximate the derivative y by backward differences of the y-values.

In a k-step BDF-method the solution is approximated by a polynomial P^C_{n+1} of order k, that fulfills the following conditions:

Given already values for the solution at the last k time points $t_n, \ldots, t_{n+1-k}$ the polynomial is required to interpolate the computed solution at these points

$$P^C_{n+1}(t_{n+1-i}) = y_{n+1-i}, \quad i = 1, \ldots, k,$$

and its derivative is equal to the right-hand side of the ODE

$$P^C_{n+1}(t_{n+1}) = f(t_{n+1}, P^C_{n+1}(t_{n+1}))\,.$$

The value at the actual time point t_{n+1} is then given by

$$P^C_{n+1}(t_{n+1}) = y_{n+1}.$$

These $k+1$ conditions define a unique polynomial of degree k.

Thus, in every step of the integration, one must solve

$$P^C_{n+1}(t_{n+1}) =: -\frac{1}{h}(\alpha_0 y_{n+1} + cc) = f(t_{n+1}, y_{n+1})\,, \tag{34}$$

with cc the constant part of the corrector polynomial except the unknown y_{n+1}.

This set of nonlinear equations is implicit and has to be solved by an iterative method, like Newton's method, which has been proved good for stiff systems.

Solving the nonlinear system (34) via Newton iteration requires a starting guess $y^{(0)}_{n+1}$ (predictor). This is obtained by evaluating a polynomial P^P_{n+1} which interpolates the last, already given $k+1$ y-values

$$P^P_{n+1}(t_{n+1-i}) \;=\; y_{n+1-i}, \quad i = 1, \ldots, k+1,$$

at the point t_{n+1}

$$P^P_{n+1}(t_{n+1}) \;=\; y^P_{n+1}\,.$$

The polynomial $P^P_{n+1}(t)$ extrapolating the values $y_n, \ldots, y_{n+1-k}$ is given by

$$P^P_{n+1}(t_{n+1}) = \sum_{i=0}^{k} p_i(t_{n+1})\nabla^i y_n$$

with

$$p_i(t) = \begin{cases} 1 & i = 0 \\ \prod_{j=1}^{i}(t - t_{n+1-j}) & i = 1, \ldots, k+1 \end{cases}$$

and the divided differences

$$\nabla^0 y_n \;=\; y_n \tag{35}$$

$$\nabla^i y_n \;=\; \frac{\nabla^{i-1} y_n - \nabla^{i-1} y_{n-1}}{t_n - t_{n-i}}\,. \tag{36}$$

Instead of the divided differences itself so-called modified divided differences are stored. This reduces the expense of updating and storing the coefficients from step to step.

To denote the predictor and corrector polynomials P^P_{n+1} and P^C_{n+1} in terms of modified divided differences we have to introduce the following quantities:

$$\psi_j(n+1) \;=\; t_{n+1} - t_{n+1-j} = \psi_{j-1}(n) + h_{n+1}$$

$$\beta_j(n+1) \;=\; \frac{\psi_1(n+1)\cdot\ldots\cdot\psi_{j-1}(n+1)}{\psi_1(n)\cdot\ldots\cdot\psi_{j-1}(n)}, \quad \beta_j(1) = 1$$

$$\gamma_j(n+1) \;=\; \sum_{i=1}^{j} \frac{1}{\psi_i(n+1)}$$

The modified divided differences are of the form

$$\Phi^*_j(n) \;=\; \psi_1(n+1)\cdot\ldots\cdot\psi_{j-1}(n+1)\nabla^{j-1} y_n$$

and

$$\delta_j(n+1) \;=\; \sum_{i=1}^{j} \Phi^*_i(n)\,.$$

denotes the sum of them.

The predictor is then given by

$$y^P_{n+1} \;=\; y_n + \sum_{j=1}^{k} \Phi^*_{j+1}(n)$$

and for the corrector we have

$$\begin{aligned} y^C_{n+1} \;&=\; P^C_{n+1}(t_{n+1}) \\ &=\; h_{n+1}\gamma_{k+1}(n+1)y^C_{n+1} - cc \end{aligned}$$

with

$$cc = \sum_{j=1}^{k} \frac{1}{\psi_j(n+1)}\delta_j(n+1)\,. \tag{37}$$

From step to step only the quantities ψ_j and δ_j have to be stored. (For a detailed description of the predictor and corrector polynomials see, e.g., Brenan et al. (1989), Eich (1991)).

6.2. Error estimation and stepsize control

Because the global error is not easily accessible, error control of integration methods is based on estimates of the local error. In contrast to other solvers the error estimates in DAESOL are made on variable grids.

In the following we describe the error estimation and step size selection for DAESOL based on the quantities given above.

6.2.1. Error estimation

The local error of a discretization method is defined by the difference between the exact solution of the differential equation inserted into the difference equation and the solution itself. In a BDF-method of order k in step $n+1$ we choose an estimate for the local error

$$E_k(n+1) = \frac{h_{n+1}}{h_{n+1}\gamma_{k+1}(n+1)} \cdot \psi_1(n+1)\cdot\ldots\cdot\psi_k(n+1)\cdot\|\nabla^{k+1}y_{n+1}\|\,. \tag{38}$$

After every step we check this error formula. If the estimated error $E_k(n+1)$ is bigger than a tolerance TOL, TOL a prescribed value given by the user, the step is rejected and the step size has to be reduced. The step size reduction after rejected steps is described in detail at the end of this chapter.

The error in the next step of integration depends on the one hand on the discretization of the BDF-method and on the other hand on evaluating only an approximate solution. The first one is the main part of the error and in the following we will only take this one into consideration.

With the error in step $n+1$ equal to (38), the accumulated error in step $n+2$ is of the form

$$\begin{aligned} E_k(n+2) &= \frac{h_{n+2}}{h_{n+2}\gamma_{k+1}(n+2)} \cdot\psi_1(n+2)\cdot\ldots\cdot\psi_k(n+2)\cdot\|\nabla^{k+1}y_{n+2}\| \\ &= \frac{h_{n+2}^2}{h_{n+2}\gamma_{k+1}(n+2)}\cdot q(h_{n+2})\cdot\left[\|\nabla^{k+1}y_{n+1}\| + (\psi_{k+2}(n+2)+\psi_{k+1}(n+2))\cdot\|\nabla^{k+2}y_{n+1}\|\right] \end{aligned} \tag{39}$$

with

$$q(h_{n+2}) = (h_{n+2}+\psi_1(n+1))\cdot\ldots\cdot(h_{n+2}+\psi_{k-1}(n+1))\,.$$

6.2.2. Step size and order selection

The step size should be determined such that

$$E_k(n+2)\le TOL.$$

Because it is very difficult to estimate a new step size from formula (39), most solvers use a simplified error formula and proceed as follows:

The analogue to formula (38) on equidistant grids is

$$\hat{E}_k(n+1) := \frac{1}{h_{n+1}\gamma_{k+1}(n+1)}\cdot k!\,h^{k+1}\|\nabla^{k+1}y_{n+1}\|\,.$$

With $\hat{E}_k(n+1)\le\widehat{TOL}$ one obtains the new step size

$$\hat{h} = \sqrt[k+1]{\frac{h\gamma_{k+1}(n+1)\cdot\widehat{TOL}}{k!\,\|\nabla^{k+1}y_{n+1}\|}}\,. \tag{40}$$

To estimate a new step size and order this formula is evaluated for different orders $k'=k-1,k,k+1$ with $TOL<\widehat{TOL}$, e.g., $\widehat{TOL}=\frac{1}{2}\cdot TOL$. We increase or decrease the order by one if the calculated step size according to this order is significantly bigger than the one according to the order in the last step. Otherwise the order is retained.

But formula (40) seems to be unsuitable for the computation with changing step sizes. On the one hand it is based on error formulas on variable grids (factor $\gamma_{k+1}(n+1)$) and on the other hand the step size is regarded as to be constant ($(k+1)$-st root).

Therefore DAESOL uses a different strategy for step size control:

First also the maximal step size $\hat{h}$ is chosen in the previous mentioned damped way. For the next step the chosen step size should fulfill the non-equidistant error formula (39):

$$\begin{aligned} E_k(n+2) &= \frac{h^2}{h_{n+2}\gamma_{k+1}(n+2)}\cdot q(h)\cdot\left[\|\nabla^{k+1}y_{n+1}\| + (\psi_{k+2}(n+2)+\psi_{k+1}(n+2))\cdot\|\nabla^{k+2}y_{n+1}\|\right] \\ &\le TOL. \end{aligned} \tag{41}$$

If that is true, the step size is accepted, otherwise it will be reduced (by the way of formula (41)):

$$h^2 = \frac{1}{q(h^*)}\cdot \frac{h\gamma_{k+1}(n+2)\cdot TOL}{\left[\|\nabla^{k+1}y_{n+1}\| + (\psi_{k+2}(n+2)+\psi_{k+1}(n+2))\cdot\|\nabla^{k+2}y_{n+1}\|\right]} \tag{42}$$

with h^* the previously chosen step size (see also Bock et al. 1995).

The order and step size control with step size selection based on variable grids and released order leads to more reliability and on an average to less rejected steps, which was shown by Bleser (1986) for the examples of *STIFF DETEST* (Enright et al. 1975).

6.2.3. Scaling

The variables of the solution are often of different magnitude. To take this into account, e.g., for error control, a weighted norm is used instead of the l_2-norm $\|y\|_2$

$$\|y_n\| = \frac{1}{m}\sqrt{\sum_{i=1}^{m}\left(\frac{y_n(i)}{yscal_n(i)}\right)^2}$$

with $yscal_n(i) = max\,(|y_n(i)|, yscal_{n-1}(i), atol(i))$.

$atol$ may be a scalar or a vector. For problems whose solution components are scaled very differently from each other it is advisable to provide the tolerances vector valued. With the value $atol(i)$ one can weight component i of y. Components which are

less than $atol(i) \cdot TOL$ will not be considered for error control in the integration. This simple measure will save a lot of run time.

The scaling described above is not the only one availabe for DAESOL but the one used for the numerical results in this paper. It is useful for stiff systems where one is not so much interested in small solution components fading away very fast.

6.3. Solution of the nonlinear system - monitor strategy

The BDF-code DAESOL solves initial value problems for DAEs of the following rather general linear implicit form

$$\begin{aligned} A(t,y,z)\,y &= f(t,y,z) \\ 0 &= g(t,y,z), \quad y(t_0) = y_0, \end{aligned} \tag{43}$$

whereas $A(t,y,z)$ and $\frac{\partial g}{\partial z}$ are assumed to be regular (A may be the identity). The DAE is then said to be of index 1 (for a further description of the index definition see, e.g., Brenan et al. 1989).

Inserting the BDF-formulas in (43) results in

$$\begin{aligned} A(t_{n+1}, y_{n+1}, z_{n+1})(\alpha_0 y_{n+1} + cc) &= -h\, f(t_{n+1}, y_{n+1}, z_{n+1}) \\ 0 &= g(t_{n+1}, y_{n+1}, z_{n+1})\,. \end{aligned} \tag{44}$$

This system defines implicitly the unknown $x_{n+1} = (y_{n+1}, z_{n+1})$. We obtain an estimate x^P_{n+1} for all components of x_{n+1} from the predictor polynomial. This estimate is an initial guess for the Newton-like method, used to solve the nonlinear system.

Defining (44) shortly as

$$F(x_{n+1}) = 0, \qquad \text{with} \quad x_{n+1} = (y_{n+1}, z_{n+1})$$

a Newton-step is given by

$$x^{(m+1)}_{n+1} = x^{(m)}_{n+1} + \Delta x^{(m+1)}_{n+1}$$

whereas $\Delta x^{(m+1)}_{n+1}$ solves the linear system of equations

$$J(x^{(m)}_{n+1}) \cdot \Delta x^{(m+1)}_{n+1} = -\,F(x^{(m)}_{n+1}),$$

with

$$J(x^{(m)}_{n+1}) = \begin{pmatrix} \alpha_0 A + A_y cc + h\, f_y & A_z cc + h\, f_z \\ g_y & g_z \end{pmatrix}$$

the Jacobian of F and with cc the constant part of the corrector polynomial approximating y_{n+1}, defined in (37).

For many applications, especially when the system is large or the functions of the DAE are very complex, evaluation and decomposition of the Jacobian J takes most part of time of the integration. In general the Jacobian J changes very little during the Newton iteration and even during several steps of integration. In order to save computing time, it is advisable to keep the decomposition of J frozen as long as possible, but, on the other hand, freezing the Jacobian impairs the convergence ratio of the Newton-like method.

In the following we describe a monitor-strategy that is designed to reduce the total computational effort for the integration by freezing the Jacobian as long as possible.

Convergence of the Newton-like method holds on the following assumptions (Bock 1987):

> Let $J = \frac{\partial F}{\partial x}$ be the Jacobian of F and $\tilde{J}^{-1}$ the approximate inverse of J. For all $\tau \in [0,1]$ and all m there are bounds ω and κ such that
>
> $$\begin{aligned} &\|\tilde{J}^{-1}(x^{m+1})(J(x^m) - J(x^m - \tau\Delta x^m)) \cdot \Delta x^m\| \\ &\qquad \le \omega^m \tau \|\Delta x^m\|^2, \quad \omega^m \le \omega < \infty \end{aligned}$$
>
> $$\begin{aligned} &\|\tilde{J}^{-1}(x^{m+1})(F(x^m) - J(x^m)\tilde{J}^{-1}(x^m)F(x^m))\| \\ &\qquad \le \kappa^m \|\Delta x^m\|, \quad \kappa^m \le \kappa < 1 \end{aligned}$$
>
> and the starting point of the iteration has to fulfill
>
> $$\delta_0 := \frac{\omega^0}{2}\|\Delta x^0\| + \kappa^0 < 1\,. \tag{45}$$
>
> Then the iteration converges with
>
> $$\|\Delta x^{m+1}\| \le (\frac{\omega^m}{2}\|\Delta x^m\| + \kappa^m)\|\Delta x^m\| \le \|\Delta x^m\|$$
>
> and for the m-th iterated there is an a priori estimate
>
> $$\|x^m - x^*\| \le \|\Delta x^0\| \frac{\delta_0^m}{1-\delta_0}\,. \tag{46}$$

ω denotes the nonlinearity of the Jacobian J and κ is a measure for the quality of the approximate inverse $\tilde{J}^{-1}$.
After two iterations estimates about the behaviour of the convergence ratio

$$\frac{\|\Delta x^{(1)}\|}{\|\Delta x^{(0)}\|} \approx \delta_0 \tag{47}$$

can be given.

We require that maximal three Newton-iterations should be taken in order to reduce the error of the predictor sufficiently, e.g.,

$$\|x^m - x^*\| \le \|\Delta x^0\| \frac{\delta_0^m}{1-\delta_0} \le \frac{1}{12}\|\Delta x^0\|\,.$$

After two Newton-iterations we get an estimate for the convergence ratio from formula (47) and may decide whether to perform an additional Newton-step or not. If the ratio δ_0 is less than $\frac{1}{4}$, the Newton-iteration is regarded as convergent, if the ratio is less than $\frac{1}{3}$, it is regarded as convergent after one further iteration. If the ratio is bigger than $\frac{1}{3}$ the Newton-iteration failed to converge.

A poor convergence ratio respectively no convergence may have different reasons:

- a big change of the coefficients α_i of the BDF-method and of the step size h

- a big change of the matrices $\frac{\partial f}{\partial x}$, $\frac{\partial A}{\partial x}$ or $\frac{\partial g}{\partial x}$
- the predicted starting value for the Newton-method is not sufficiently close to the solution

In the first two cases, κ is too big, that means that $\tilde{J}^{-1}$ is too inaccurate. The convergence of the Newton-iteration slows down or the computed search direction for the solution is wrong. $\tilde{J}^{-1}$ should be calculated anew.

In the last case ω is too big, the starting point for the Newton-iteration does not lie in the domain of local convergence. The BDF-step has to be repeated with reduced step size.

The succession of the error causes comes up to the effort of repairing the poor convergence respectively no convergence of the Newton-method.

Therefore the procedure in DAESOL is as follows

1) As long as $\frac{\|\Delta x^1\|}{\|\Delta x^0\|} \leq \delta$, e.g., $\delta = \frac{1}{3}$, $\tilde{J}^{-1}$ is frozen.
2) If the convergence ratio is too bad, keep the matrices $\frac{\partial f}{\partial x}$, $\frac{\partial A}{\partial x}$ and $\frac{\partial g}{\partial x}$ frozen but decompose J anew with actual BDF-coefficients α_i and actual stepsize h.
3) If J is still too inaccurate, reevaluate the matrices $\frac{\partial f}{\partial x}$, $\frac{\partial A}{\partial x}$ and $\frac{\partial g}{\partial x}$ and decompose J anew.
4) If there is still no convergence repeat the step with reduced step size.

In most solvers step 2) is omitted. But experience showed that it results in one third to one half evaluations of the matrices $\frac{\partial f}{\partial x}$, $\frac{\partial A}{\partial x}$ and $\frac{\partial g}{\partial x}$.

The step size reduction in DAESOL after a failure of the convergence is based on estimates on variable grids and the step size is not only decreased, e.g., by a constant factor as in other codes. The step size should be reduced such that the Newton-method of the next step converges after two (or three) iterations. To achieve this according to the above sketched step size estimation

$$\delta_0^{(new)} \leq \frac{1}{4}$$

has to be fulfilled.

In the following we describe an estimation of the step size after rejected steps which takes the actual error into consideration.

Because the steps 1) to 4) are performed in succession, the approximate inverse $\tilde{J}^{-1}$ of the Jacobian has been evaluated and decomposed anew (in step 3)). The quantity κ is therefore 0 and so we obtain from (45)

$$\delta_0 = \frac{\omega^0}{2}\|\Delta x^{(0)}\| .$$

With

$$\delta_0^{(new)} = \frac{\omega^0}{2}\|\Delta x_{(new)}^{(0)}\| \leq \frac{1}{4}$$

we have to fulfill

$$\|\Delta x_{(new)}^{(0)}\| \leq \frac{\|\Delta x^{(0)}\|}{4 \cdot \delta^0} .$$

Table 3. Comparison of DAESOL and DDRIV3 on the reduced model

TOL	10^{-4}		10^{-5}	
	DDRIV3	DAESOL	DDRIV3	DAESOL
steps	30 240	804	57 178	1 262
rejected steps	14 561	83	25 945	108
average order	2.23	3.07	2.08	3.12
eval. of RHS	924 072	14 239	1 705 577	21 503
eval. of Jac.	18 085	234	33 346	355
dec. of Jac.	18 085	602	33 346	898
CPU-time [s]	1 772.1	33.1	3 386.1	51.3

We estimate the new error according to error formula (38). Decreasing the tolerance TOL in this formula will implicitly reduce the step size. With E_k an approximation of $E_k(n+1)$ the error formula

$$\|E_k\| \approx \frac{1}{h\gamma_{k+1}(n+1)} \cdot \frac{h}{t_{n+1} - t_{n-k}} \cdot \|\Delta x^{(0)}\|$$

should require $\|E_k\| \leq TOL'$ instead of $\|E_k\| \leq TOL$, with

$$TOL' = \frac{1}{h\gamma_{k+1}(n+1)} \cdot \frac{h}{t_{n+1} - t_{n-k}} \cdot \frac{\|\Delta x^{(0)}\|}{4 \cdot \delta^0} .$$

Inserting TOL' in (38) instead of TOL will lead to

$$\delta_0^{(new)} \leq \frac{1}{4} .$$

7. Results and interpretation

We followed the chemical evolution in a gas element which moves from a large initial radius towards the centre of the disk. The temperature and pressure both strongly increase and this causes strong changes in the chemical composition of a specific gas parcel in the course of time.

7.1. Numerical results

To show the efficiency of the integrator we compare DAESOL with DDRIV3 (Kahaner et al. 1989), a code that is widely used for the solution of initial value problems in astrophysics. The code is also a multistep-method based on Backward Differentiation Formulae, but with different strategies in error control and order and step size selection.

For the comparison we consider a reduced model with 46 species and with the opacity κ and the mean molecular weight μ held constant. This leads to a system of 46 differential equations.

Table 3 shows the comparison of the two codes from the beginning of the integration (1000 AU) to 0.56 AU with different achieved accuracies TOL. The system was computed on an SGI Indy with a R4600 processor.

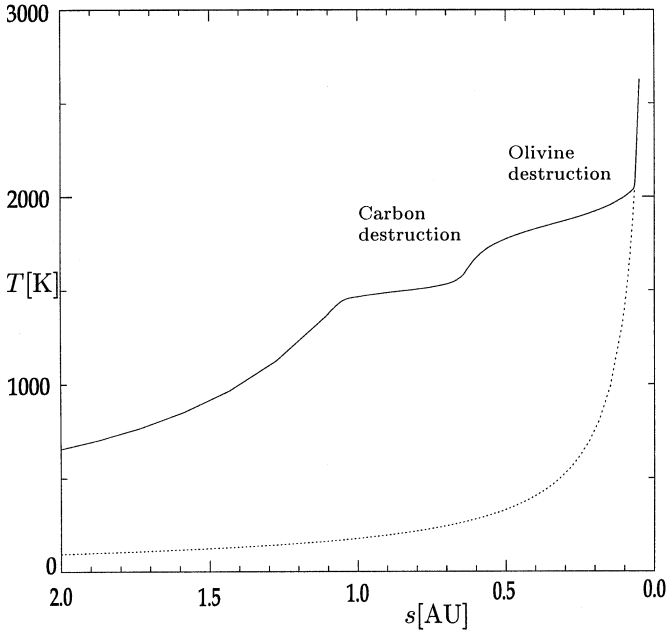

Fig. 1. Radial run of midplane temperature in the accretion disk. The full line shows the result of the model calculation. The dotted line shows, for comparison, the run of temperature in a model without dust.

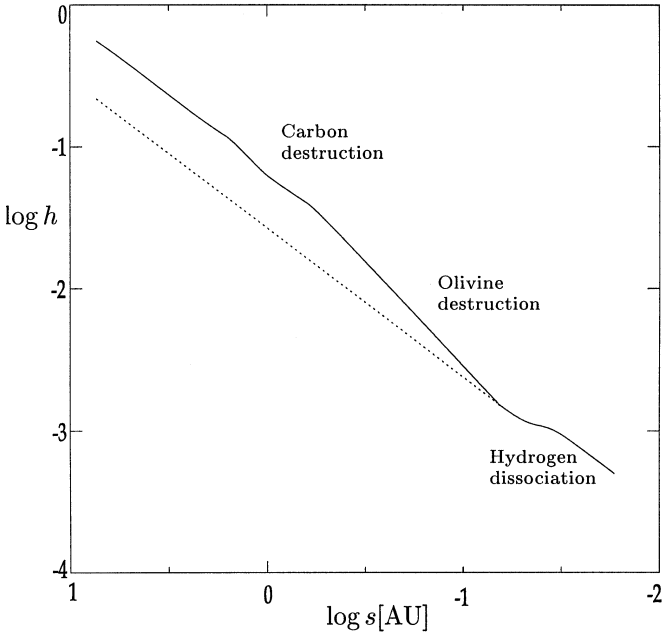

Fig. 2. Radial run of disk height (in units AU) in the accretion disk. The full line shows the result of the model calculation. The dotted line shows, for comparison, the disk height in a model without dust.

For DDRIV3 the number of steps taken and of rejected steps increases rapidly when higher accuracies have to be achieved, which is also reflected in the long run-times.

To avoid instabilities order and step size in DDRIV3 are fixed for at least $k+1$ steps. This results in an average order of about one lower than for DAESOL, where order and step size may change in every step.

Also the number of function evaluations differs very much. The higher number of steps in DDRIV3 is not the only reason but also the monitor strategy in DAESOL which reduces the number of evaluations of the Jacobian needed for the Newton-method.

7.2. Disk structure

The general structure of the protoplanetary disk turns out to be very similar to that obtained in paper I, since the disk structure does not strongly depend on the details of the chemistry. The essential process is the mutual coupling between dust absorption, temperature and vaporization of the last dust component. Details of the disk structure, however, change.

Fig. 1 compares the central plane temperature in the accretion disk for two models, one with dust and the other without taking dust opacities into account. The dotted line indicates the case of no dust opacity i.e. only with an assumed Rosseland mean opacity of 0.001 $\mathrm{cm}^2 \cdot \mathrm{g}^{-1}$ for the gas phase. The radial distribution of temperature in the disk model shows two plateaus corresponding to the evaporation of the carbon dust in the region between ≈ 1 and ≈ 0.5 AU and of the olivine dust in the region between ≈ 0.5 and ≈ 0.1 AU. They are caused by the decrease of opacity in the course of dust evaporation which counteracts the temperature increase with decreasing radius. When all dust particles have disappeared, the two temperature curves join.

As in paper I we observe the reduction in the thickness of the accretion disk due to dust destruction and the short plateau due to the change in the mean molecular weight because of H_2 dissociation (cf. Fig. 2). There is one essential difference, however. The molecular hydrogen dissociation occurs in the protoplanetary accretion disk in a state far from equilibrium. The rather high particle density results in efficient H-H-recombination to H_2 which is not readily compensated by collisional dissociation. This shifts the region of hydrogen dissociation from around ≈ 0.25 AU in a model based on chemical equilibrium down into a region of higher temperature around $s \approx 0.05$ AU. The degree of dissociation of hydrogen in the protoplanetary disk is less than in chemical equilibrium.

7.3. Molecules in the gas phase

Fig. 3 shows the chemical composition of the gas phase in the disk's central plane in the region where carbon and silicate dust evaporates. The initial composition changes only slightly. At $s \approx 21$ AU where $T \approx 30$ K the CO ice evaporates and introduces CO into the gas phase. At ≈ 8 AU where $T \approx 150$ K the water ice evaporates and introduces H_2O into the gas phase. The initially assumed 1% fraction of free H atoms drops to a very low level due to H_2 formation by three body collisions. Ternary reactions are efficient in the protoplanetary disk due to its high particle density and the rather long available reaction time of the order of 10^5 yr. This simple composition of the gas phase (mainly H_2, H_2O, CO, N_2) prevails until the temperature of the inwards moving gas parcel has climbed to a temperature

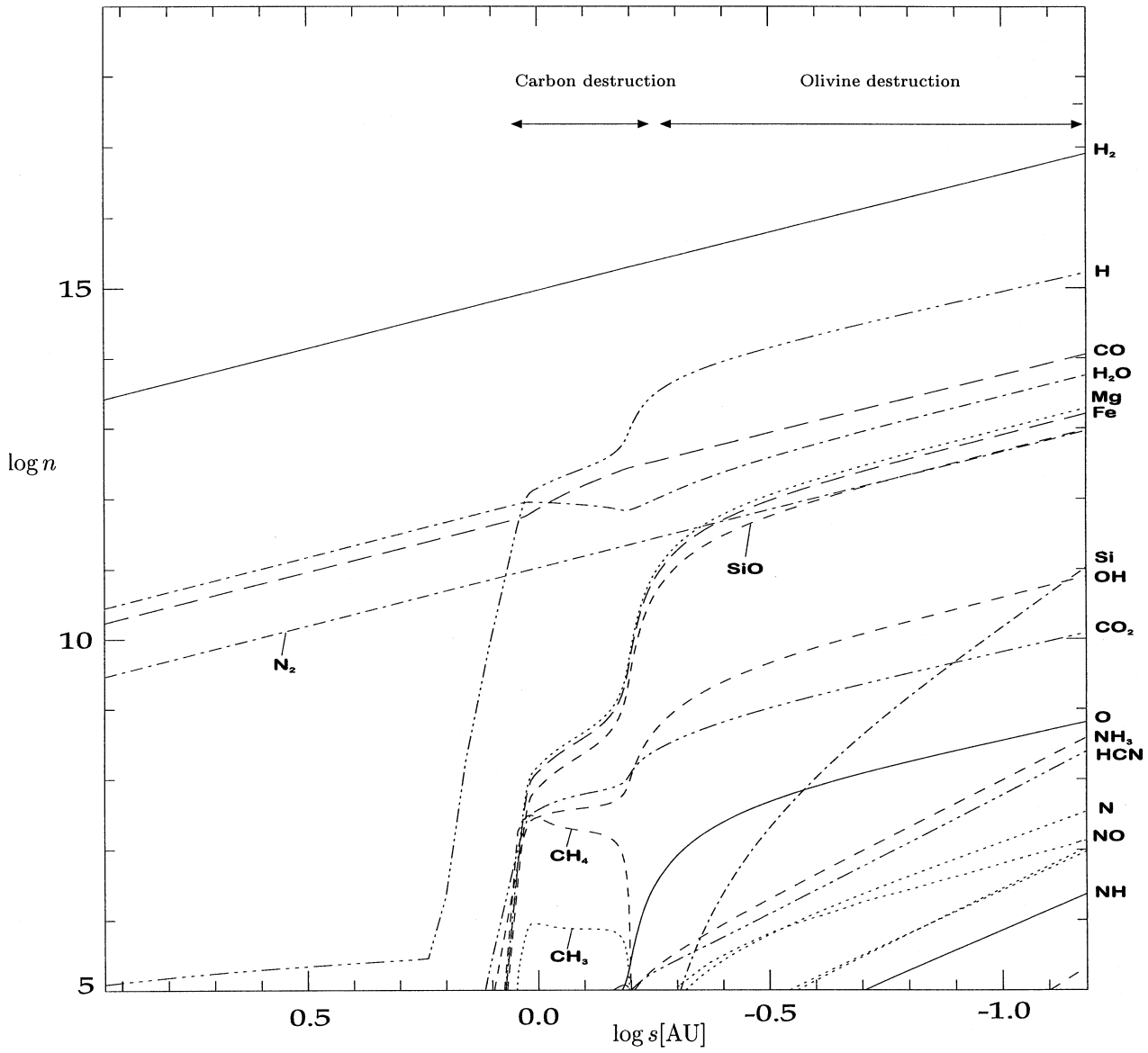

Fig. 3. Run of molecular abundances in the accretion disk in the region of dust destruction.

of $\approx$ 1000 K and collisional H dissociation and dust evaporation sets in.

7.3.1. Carbon vaporization

Carbon dust evaporates first in the radius regime between 1 and 0.5 AU where $T \approx 1\,200 \ldots 1\,300$ K. This results in an increase of the CO abundance in the gas phase since CO is the most stable carbon compound in an oxygen rich element mixture at elevated temperatures. The conversion of the carbon into CO requires several intermediate chemical reaction steps. In the course of this process, the evaporated carbon atom reacts in the gas phase first with the abundant H and forms the hydrocarbon molecules CH_i ($i = 1, \ldots 4$). Due to the high H_2 abundance the hydrogen addition reactions

$$CH_i + H_2 \longrightarrow CH_{i+1} + H$$

proceed faster than the hydrogen abstraction reactions

$$CH_{i+1} + H \longrightarrow CH_i + H_2$$

and most of the carbon injected into the gas phase accumulates in CH_4 and a small fraction in CH_3, CH_2, CH. These simple hydrocarbons are found with noticeable abundances as temporary products of carbon destruction at $s \approx 1$ (cf. Fig. 3).

The oxidation of the hydrocarbons has to occur by reaction with an oxygen bearing compound. The abundant water molecule does react with the CH_i via

$$CH_i + H_2O \longleftrightarrow CH_{i+1} + OH\,.$$

This reaction is fast in both directions but has practically no influence on the abundance of CH_i, since it cannot compete with the more frequent reactions with hydrogen. Direct oxidation reactions of the hydrocarbons with the water vapor are known

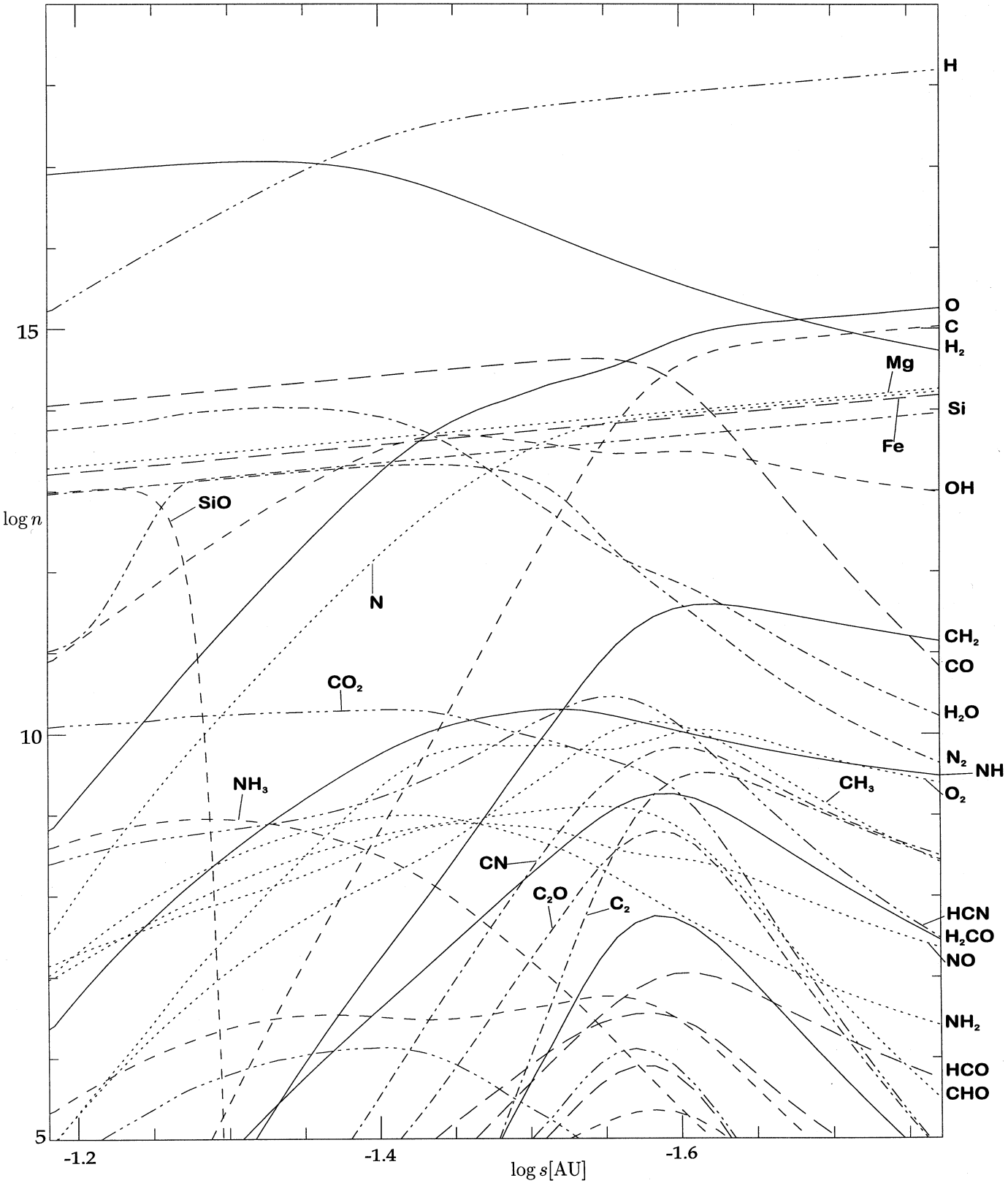

Fig. 4. Run of molecular abundances in the accretion disk in the innermost region of molecule dissociation.

from flame chemistry to be inefficient. Oxidation reactions occur for hydrocarbons with OH and O (Warnatz 1981, 1983) which are present in the gas phase as dissociation products of water[5]:

$$CH_3 + O \longrightarrow CH_2O + H$$

and

$$CH_2 + OH \longrightarrow CH_2O + H\,.$$

The formaldehyde reacts with H to form the formyl radical

$$CH_2O + H \longrightarrow CHO + H_2$$

and this reacts again with H to form CO

$$CHO + H \longrightarrow CO + H_2\,.$$

A different possible pathway to CO goes through the condensation reaction

$$CH_3 + CH_3 \longrightarrow C_2H_4 + H_2\,.$$

The C_2H_4 looses in a series of reactions with H its hydrogen atoms

$$C_2H_i + H \longrightarrow C_2H_{i-1} + H_2\,.$$

until the ethynyl radical C_2H is formed. This finally reacts with O to form CO

$$C_2H + OH \longrightarrow CO + CH_2\,.$$

These main reaction paths for the oxidation of the methane are shown schematically in Fig. 5. They are just the same in the accretion disk as in the combustion of hydrocarbons.

A lot of additional reactions occur besides these ones in the conversion of the intermediate product CH_4 into the final product CO. More details will be discussed in a different paper (Finocchi et al. 1996). The present results for the gas phase chemistry are somewhat modified if carbon oxidation is considered (Finocchi et. al. 1996a).

7.3.2. Olivine evaporation

Between 0.5 and 0.1 AU ($T \approx 1\,500 \ldots 1\,600$ K) the olivine dust particles evaporate and eventually are destroyed. This injects Mg, Fe, SiO, and O into the gas phase. The evaporation of the last dust component (in our case the olivine) is in numerical respect the most critical one for solving the DAE system. The strong nonlinear coupling between temperature, dust opacity and dust evaporation and the very strong variation of physical timescales over small temperature intervals makes it a hard task to solve this problem numerically as a time dependent process. In paper I this was treated in the simplifying approximation of a quasistationary vaporization, which sails round most of the problems occurring in the time dependent case. Attempts to solve this problem with known algorithms for stiff problems failed. The algorithm finally used in this calculation, which is discussed in Sect. 6, turned out to work fine without any problems.

[5] In laboratory methane combustion they result from dissociation or reaction of O_2.

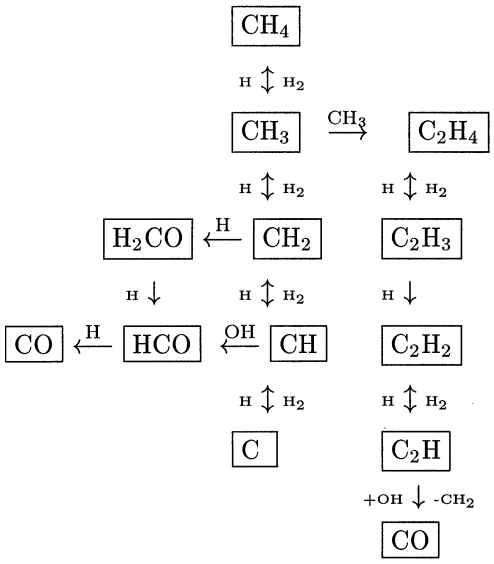

Fig. 5. A chemical pathway for CO formation

The vaporization of the silicate injects besides the metals Mg and Fe the molecule SiO and the atom O into the gas phase. In our current calculations Fe and Mg remain unchanged because no reactions of these species are taken into account as yet. The SiO is dissociated later, at a higher temperature, by collisions with H_2 and H yielding Si and O in the gas phase. The free oxygen atoms injected into the gas phase forms H_2O according to the two following reactions

$$O + H_2 \longrightarrow OH + H$$

and

$$OH + H_2 \longrightarrow H_2O + H$$

Fig. 4 shows the inner part of the protoplanetary disk in which a huge number of different molecular species occurs. This is due to the fact that at temperatures above 1 500 K many reactions become possible which are kinetically forbidden at lower temperatures. Most of the molecules dissociate at radii below ≈ 0.06 AU. Dissociation of molecular hydrogen occurs at ≈ 0.05 AU. Close to the centre of the disk the temperature increases so much that only the free atoms C, H, O, N, Mg, Fe, and Si remain.

8. Summary

We have investigated the gas phase chemistry in a protoplanetary accretion disk. In doing so we have concentrated on that aspects of gas phase chemistry that is initiated by destruction of dust in the vicinity of the accreting young star.

For handling the stiffness of the system of DAEs for this problem, together with the huge changes of the rate coefficients resulting from the wide range of temperatures, we have presented and discussed a new BDF-method for the integration of the equation system (Sect. 6). We find that the corresponding numerical code DAESOL is more robust and faster than the code used originally (Duschl et al. 1996), by typically a factor of ≈ 30 in CPU time on otherwise identical systems.

The accretion disk was assumed to be in a stationary phase of its evolution. We have used a semi-analytical description based on the standard models for accretion disks (Sect. 2). For the chemical aspect of the disk models, we considered explicitly the reaction kinetics under the conditions of a protoplanetary disk (Sect. 3). We mainly took into account the four most abundant elements, H, C, N, and O. The dust at large radii was modelled as a mixture of C- and of Fe-Mg-Si-dust with H_2O and CO in the dust grains' ice mantles (Sect. 4). In addition to the formation and dissociation of molecules, we allowed for vapourisation of the ice mantles and for destruction of the dust thus linking the evolution of the gas and of the dust phases in the disk. The direct coupling between the accretion disk structure and the description of the chemistry manifests itself in the opacity coefficient κ through its dependence on temperature, density and chemical composition of the disk matter (Sect. 5).

While the general features of the disk structure are very similar to what Duschl et al. (1996) find for the case without explicit consideration of the gas phase chemistry, details that may be important for planetary evolution change considerably (Sect. 7). This is mainly due to deviations from chemical equilibrium.

We observe dust destruction in the radial range of $\approx 1 \ldots 0.5$ AU for carbon dust and between ≈ 0.5 and 0.1 AU for olivine dust. Under the more realistic dust/gas coupling, hydrogen dissociation occurs at smaller radii (≈ 0.05 AU) than in previous models (c.f., Duschl et al. 1996: ≈ 0.25 AU). For radii < 0.05 AU all molecules are dissociated leaving only free atoms C, H, O, N, Mg, and Si in our protoplanetary accretion disk.

Acknowledgements. We grateful acknowledge stimulating discussions with W. M. Tscharnuter, J. Warnatz and especially H. G. Bock, who has decisively influenced the development of DAESOL over the last 10 years. This work has been supported by the Deutsche Forschungsgemeinschaft (DFG), Sonderforschungsbereich 359 " Reaktive Strömungen, Diffusion und Transport".

References

Alexander D.R., Ferguson J.W., 1994, ApJ 437, 879
Anders E., Grevesse N., 1989, Geochimica et Cosmochimica Acta 53, 197
Bauer I., 1994, Numerische Behandlung Differentiell-Algebraischer Gleichungen mit Anwendungen in der Chemie, Master's thesis, Universität Augsburg
Baulch D.L., Cobos C.J., Cox R.A., Esser C., Franck P, Just Th., Ker J.A., Pilling M.J., Troe J., Walker R.W., Warnatz J., 1992, Journal of physical and chemical reference data 21, 411
Beck H., 1993, Ionization, Chemistry, and Dust formation in the Outflows of Classical Novae and Red Giants, PhD thesis, Technische Universität Berlin
Beckwith S.V.W., Sargent A.I., 1993, in Protostars and Planets III, E.H. Levy and J.I. Lunine Eds., University of Arizona Press, Tuscon, p. 521
Bleser G., 1986, Eine effiziente Ordnungs- und Schrittweitensteuerung unter Verwendung von Fehlerformeln für variable Gitter und ihre Realisierung in Mehrschrittverfahren vom BDF-Typ, Masters's thesis, Universität Bonn
Bock H.G., 1987, Bonner Mathematische Schriften 183
Bock H.G., Schlöder J.P., Schulz V.H., 1995, Numerik großer Differentiell-Algebraischer Gleichungen. Simulation und Optimierung, in Prozeßsimulation, H. Schuler ed., Verlag Chemie, Weinheim
Brenan K.E., Campbell S.L., Petzold L.R., 1987, Numerical Solution of Initial-Value Problems in Differential-Algebraic Equations, North Holland, New York
Cameron A.G.W., 1973, Space. Sci. Rev. 15,122
Cameron A.G.W., 1988, ARA&A 26, 441
Curtiss C.F., Hirschfelder J.O., 1952, Proc. Nat. Acad. Sci. 38, 235
Dolginov A.Z., Stepinski T.F., 1994, ApJ 427, 377
Dorschner J., Henning T., A&AR 6, 271
Draine B.T., 1985, ApJS 57, 587
Draine B.T., Lee H.M., 1984, ApJ 285, 89
Duschl W.J., Gail H.-P., Tscharnuter W.M., 1996, A&A (in press) (paper I)
Eich E., 1987, Numerische Behandlung semi-expliziter differentiell--algebraischer Gleichungssysteme vom Index 1 mit BDF-Verfahren, Master's thesis, Universität Bonn
Eich E., 1991, Projizierende Mehrschrittverfahren zur numerischen Lösung von Bewegungsgleichungen technischer Mehrkörpersysteme mit Zwangsbedingungen und Unstetigkeiten, VDI-Verlag, Düsseldorf, Dissertation, Universität Augsburg, published as Fortschr.-Ber. VDI Reihe 18 Nr. 109
Elmegreen B.G., 1978, Moon and Planets 19, 261
Enright W.H., Hull E.T., Lindberg B., 1975, BIT 15
Finocchi F., Gail H.-P., Duschl W.J., Tscharnuter W.M., 1996, Proceedings of IAU Colloquium 150 (in press)
Finocchi F., Gail H.-P., 1996, (in preparation)
Franck J., King A., Raine D., 1992, Accretion power in astrophysics, Cambridge University Press, 2nd Ed.
Gear C.W., 1971, IEEE Trans. Circuit Theory, CT-18, 89
Horedt G.P., 1978, A&A 64, 173
Kahaner D., Moler C., Nash S., 1989, Numerical methods and software, Englewood Cliffs, Prentice-Hall
Léger A., Jura M., Omont A, 1985, A&A 144, 147
Lenzuni P., Gail H.-P., Henning Th., 1995, ApJ 447, 848
Lissauer J.J., 1993, ARA&A 31, 129
Lynden-Bell D., Pringle J.E., 1974, MNRAS 168, 603
Mathieu R.D., 1994, ARA&A 32, 465
Mathis J.S., Rumpl W., Nordsieck K.H., 1977, ApJ 217, 425
Mitchell G.F., 1984, ApJS 54, 81
Neufeld D.A., Hollenbach D.J., 1994, ApJ 428, 170
Pollack J.B., Hollenbach D., Beckwith S., Simonelli D.P., Roush T., Fong W., 1994, ApJ 421, 615
Prinn R.G., 1993, in Protostars and Planets III, E.H. Levy and J.I. Lunine Eds., University of Arizona Press, Tuscon, p. 1005
Pruppacher H.R., Klett J.D., 1978, Microphysics of Clouds and Precipitation, Reidel, Dordrecht
Ruden S.P., Pollack J.B., 1991, ApJ 375, 740

Sandford S.A., Allamandola L.J., 1988, Icarus 76, 201
Sandford S.A., Allamandola L.J., 1993, ApJ 417, 815
Strom S.E., Edwards S., Skrutskie M.F., 1993, in Protostars and Planets III, E.H. Levy and J.I. Lunine Eds., University of Arizona Press, Tuscon, p. 837
Swindle T.D., 1993, in Protostars and Planets III, E.H. Levy and J.I. Lunine Eds., University of Arizona Press, Tuscon, p. 867
Umebayashi T., Nakano T., 1981, PASJ 33, 617
van Dishoek E.F., Blake G.A., Draine B.T., Lunine J.I., 1993, in Protostars and Planets III, E.H. Levy and J.I. Lunine Eds., University of Arizona Press, Tuscon, p. 163
Warnatz J., 1981, Eighteenth Symposium (International) on Combustion, The Combustion Institute, p. 369
Warnatz J., 1983, Ber. Bunsenges. Phys. Chem. 87, 1008
Weast R.C., Astle M.J., 1982, CRC Handbook of Chemistry and Physics, 62nd Ed., CRC Press, Boca Raton

This article was processed by the author using Springer-Verlag LaTeX A&A style file *L-AA* version 3.